MDPI

Article

Preparation of Activated Carbon from Korean Anthracite: Simultaneous Control of Ash Reduction and Pore Development

Seokhwi Kim [1,*], Sang-Eun Lee [1], Seung-Han Baek [2], Uikyu Choi [2] and Hyo-Jin Bae [2]

[1] Center for Bio-Resource Recycling, Institute for Advanced Engineering, Yongin 11780, Republic of Korea; lse9907@iae.re.kr
[2] Korea Mine Rehabilitation and Mineral Resources Corporation, Wonju 26464, Republic of Korea; shbaek@komir.or.kr (S.-H.B.); ukchoi@komir.or.kr (U.C.); hjn496@komir.or.kr (H.-J.B.)
* Correspondence: shkim5526@iae.re.kr

Abstract: Anthracite stands as a valuable precursor for carbon materials, owing to its high carbon content. However, producing activated carbon from anthracite presents significant challenges due to its elevated ash content (23–40 wt%) and crystalline nature. The high ash content not only fails to contribute to the activation process but also obstructs pore formation on the carbon surface. To address these challenges, this study explores the preparation of activated carbon from anthracite using KOH activation. This method demonstrates remarkable efficacy in enhancing reactivity beyond the inherent physical properties of anthracite. In contrast to physical activation, the utilization of KOH as a chemical agent substantially enhances the specific surface area, resulting in a production yield of 62% and a specific surface area that reaches up to 1596 m^2/g at a KOH/anthracite weight ratio of 4.0. Moreover, rinsing the activated sample with tap water achieves an ash removal rate of about 37.9%, surpassing twice the rate achieved through acid pretreatment (67.0%). A noteworthy observation from this study is the substantial reduction in the content of major ash components, such as silicon (Si) and aluminum (Al), both of which are prominent constituents in anthracite ash. Following KOH activation, their levels decrease by approximately 54% to 65%, respectively. These findings highlight the potential of utilizing available anthracite, even with elevated ash content, as a superior carbon material. Fundamentally, the KOH activation method serves a dual purpose: it effectively reduces ash content and promotes pore creation within a highly alkaline environment. This dual advantage positions the method as a promising approach for the production of top-tier activated carbon.

Keywords: anthracite; activated carbon; activation; ash; pore development; washing

1. Introduction

Coal has been the primary energy source in the power generation industry. However, increasing global awareness of the environmental and health consequences associated with coal energy has led to a growing emphasis on exploring cleaner and alternative energy sources. Numerous studies have highlighted these critical concerns, emphasizing the necessity of transitioning towards more sustainable energy systems [1–3]. This shift towards a "fossil-free divestment" campaign extends beyond South Korea; it is evident in other coal-consuming nations like the United States and China [2,4–6]. The international community actively engages in discussions and research to discover viable solutions and innovative approaches to energy generation. These approaches aim to reduce greenhouse gas emissions and mitigate the adverse impacts of particulate pollution. This collective effort demonstrates a shared commitment to addressing the environmental, health, and economic challenges associated with coal. The ultimate goal is establishing a sustainable and cleaner energy future.

To unlock new opportunities within the coal industry and promote the growth of emerging sectors, ongoing efforts are focused on advancing coal raw material technology

while providing policy support [5,7–9]. Extensive research has been dedicated to uncovering coal's potential beyond its conventional role as a fuel, recognizing its value as a high-quality precursor. The perception of coal as a traditional industry has shifted, expanding its applications into non-conventional domains such as activated carbon [10–12] and activated carbon fibers [13,14]. Recent advancements have diversified coal's applications, transforming it into a valuable carbon-rich precursor for various nanomaterials, including graphene quantum dots (GQDs), graphene oxide, nanodiamonds, carbon nanotubes (CNTs), and more [15–21]. Zhang et al. [16] enhanced Li^+ conductivity and storage capacity by producing GQDs using high-crystallinity Taixi anthracite power with excellent thermal stability. Awasthi et al. [21] synthesized single- and multi-walled CNTs with diameters ranging from 1.2 to 1.8 nm, employing Fe and Ni–Y catalysts derived from Indian anthracite. These innovative applications not only demonstrate coal's versatility but also create opportunities for sustainable economic growth and technological advancement. By tapping into coal's potential as a valuable raw material, the objective is to revolutionize multiple industries and drive the development of cutting-edge technologies.

Traditionally, coal is categorized into distinct types based on carbonization degree: peat, lignite, bituminous coal, and anthracite. In South Korea, anthracite takes center stage in coal mining due to its high carbon content (92~98%), rendering it suitable for activated carbon production. However, the dense structure and elevated ash content of anthracite, attributed to prolonged mineralization [22], pose challenges in activated carbon manufacturing. Domestic anthracite, with an average ash content of 30% to 40%, obstructs the enhancement of derived activated carbon.

Activated carbon production involves two primary methods: chemical activation and physical activation. In chemical activation, substances like KOH, K_2CO_3, and NaOH create pores on the carbon surface, necessitating subsequent cleaning to remove residual chemicals [23–25]. On the other hand, physical activation relies on oxidizing gases such as H_2O and/or CO_2 but typically results in a lower yield. Given anthracite's high ash content and dense structure, employing a chemical agent offers the potential to optimize coal reactivity and facilitate efficient activated carbon production. Chemical activation provides a solution to the challenges posed by anthracite's ash content and dense structure, leading to the development of activated carbon with desired attributes and improved efficiency. However, even with chemical activation, it is challenging to fully eliminate ash, resulting in increased residual ash and reduced yield. Residual ash hampers pore development and diminishes specific surface area, making it difficult to produce commercially viable adsorption materials [25–27]. Ash in anthracite primarily consists of insoluble silicate minerals like kaolinite, mullite, and muscovite, which contain Si, Al, and Fe. Despite efforts to control ash content through methods like froth flotation, selectively treated coal still retains a substantial ash content of approximately 20 wt%, limiting its application as a carbon material. Various approaches have been employed to remove ash from anthracite coal as a pretreatment step [28–30], with both acid and alkali leaching methods demonstrating high treatment efficiency. Among these methods, alkaline treatment has proven particularly effective in eliminating silicate minerals.

In an alkaline environment, minerals containing Si and Al undergo demineralization, resulting in a phase transition for each metal followed by dissolution. For instance, Pan et al. attempted to extract rare earth elements like Al and Si using a roasting method with NaOH and Na_2CO_3 from coal fly ash simultaneously. Under these alkaline conditions, the mineral phase of coal fly ash, including aluminosilicate and amorphous silica, breaks down and transforms into sodium silicate and sodium aluminosilicate, both of which can dissolved in water or acid [29–31]. Additionally, Motlagh et al. [32] conducted a KOH activation reaction during the production of biochar using rice husks, which have a high ash content, as a carbon precursor. Rice husks typically contain about 12–20 wt% of Si and 30–50 wt% of carbon. The process not only recovered SiO_2 but also carbon bodies in the production of biochar. It is worth noting that the extent of dissolution may vary

depending on the specific alkali compound used, and some reactions may require elevated temperatures [31].

While KOH activation is known to effectively create pores, it has not been thoroughly discussed in terms of changes in mineral content from a mineralogical perspective. This study aims to chemically activate dense and highly crystalline anthracite using KOH to induce pore formation by triggering the dissolution of crystalline minerals present in anthracite. Consequently, we hypothesized that incorporating a cleaning process during the activation reaction can yield high-quality domestic anthracite coal. This approach not only fosters pore formation but also facilitates ash content reduction, enabling simultaneous management of anthracite's ash properties throughout the activation process.

2. Materials and Methods

2.1. Preparation of Activated Carbon from Anthracite

In this study, four types of Korean anthracite (Dogye, DG; Whasoon, JS; Jangseong, JS; Kyeongdong, KD) were utilized as carbon precursors. To address variability in ash content, a flotation-based selection technique was employed. The anthracite was first pulverized to achieve a particle size below 500 μm using a disk mill. Subsequently, a self-absorbing Denver flotation screening process was implemented, with Kelosine as a collector and pine oil as a frother. These additives were used in concentrations ranging from 20 to 25 weight percent of the mineral mixture. Specifically, 500 mg/kg of collector and 400 mg/kg of frother were added. The coal flotation test resulted in a recovery rate of approximately 75%, providing material suitable as a carbon precursor. This study explored the production of activated carbon from anthracite using both physical and chemical activation methods. In the physical activation process, steam (H_2O) was employed as the activation agent, and carbonized precursors were used. Carbonization occurred at 700 °C for 1 h, followed by heating to a formation temperature (900 °C or 1000 °C) with steam injection lasting from 0.5 to 6 h. The chemical activation approach involved activation without prior carbonization, using KOH as the agent. KOH was injected in varying amounts (1.0, 2.0, 3.0, and 4.0 weight ratios relative to anthracite) following the method described by Kim et al. [23]. The temperature was gradually raised to 850 °C in a nitrogen atmosphere at a rate of 10 °C/min until reaching the activation temperature, which was then sustained for about 3 h. After the reaction, a washing process was conducted to remove any residual alkali metal, using water and dilute hydrochloric acid until a neutral pH was achieved. The notation for anthracite-derived activated carbons was labeled in the "precursor-agent-temperature-time" format. For example, "anthracite-H-9-6H" refers to the physical activation with H_2O as activating agent at 900 °C for 6 h. Additionally, experiments were conducted to compare ash removal characteristics in anthracite. Acid leaching was performed on anthracite samples without undergoing an activation reaction. The anthracite was stirred in a 10% oxalic acid solution at 200 rpm. After stirring, the remaining ash content in the anthracite was measured following the separation of solid and liquid phases, allowing for the determination of the ash removal rate.

2.2. Analytical Methods

In this experiment, four types of anthracite underwent proximate and elemental analysis. Proximate analysis focused on volatile matter, fixed carbon, and ash content. Elemental analysis encompassed measurements of carbon, hydrogen, oxygen, nitrogen, and sulfur via an elemental analyzer (FlashSmart™, Thermo Fisher Scientific, Waltham, MA, USA). To explore the thermochemical properties of the anthracite samples, thermal weight analysis (TGA 4000, PerkinElmer, Waltham, MA, USA) was conducted. Each sample was gradually heated to 1000 °C under controlled heating rates within a nitrogen atmosphere. For a qualitative examination of the constituent minerals and the mineralogical microstructure of the anthracite, X-ray diffraction (D8 Discover GADDS, Bruker, Billerica, MA, USA) was employed. Further scrutiny of the distribution and composition of constituent elements was carried out through scanning electron microscopy with energy-dispersive X-ray spec-

trometry (SEM-EDS, Mira 3, Tescan, Brno, Czech Republic) and X-ray fluorescence (ZSX Primus-II, Rigaku, Tokyo, Japan). The primary objective of this study is to investigate alterations in the mineralogical properties of anthracite following KOH activation, utilizing XRD and SEM-EDS analysis. By examining these changes, we aim to gain insights into the mechanism responsible for reducing ash content. This analysis seeks to provide a comprehensive understanding of the ash reduction reaction mechanism during the KOH activation process. For the activated samples, specific surface area measurements were taken using N_2 adsorption (TriStar II plus, Micromeritics, NorCross, GA, USA) at a temperature of 77 K. The distribution of pores was determined by varying the relative pressure (P/P_o) of the sample after pretreatment.

3. Results and Discussion

3.1. Elemental and Chemical Compositions

Table 1 displays the results of chemical composition modifications conducted on the anthracite, both before and after froth flotation. The assessed anthracite exhibited a fixed carbon content ranging between 50 to 70 wt% and an ash content varying between 20 to 40 wt%. The carbon fraction showed an increase of approximately 20 to 30 wt% compared to the original anthracite. Notably, reductions in oxygen and sulfur contents were observed. The decreased sulfur content can be attributed to the selective influence of the floating agent used during froth flotation, designed to remove ash. Among the four types of anthracite subjected to experimentation, Si constituted the predominant component of the ash content, followed by Al and Fe, which collectively made up to 80% of the total ash composition. Although the ash content decreased after froth flotation, the proportional composition of the remaining ash within the anthracite remained notably consistent with the pre-froth flotation composition. These findings suggest that the froth flotation process primarily removed ash from the anthracite in a bulk-phase manner, using floating agents, rather than employing selective mechanisms for individual components. However, unlike other elements, the significant removal rates observed for iron (Fe) and sulfur (S) suggest potential selective removal properties of the floating agent concerning sulfide minerals.

Table 1. Chemical compositions of Korean anthracites used in this study collected from four different mines. All samples were sieved through 200 mesh before and after froth flotation, respectively.

Source		Raw Anthracite				Froth Flotation			
Sample ID		DG	WS	JS	KD	DGF	WSF	JSF	KDF
Proximate analysis (wt%)	Volatile	7.79	12.9	8.62	8.94	3.27	4.70	3.43	2.31
	Fixed carbon	61.6	51.7	50.6	67.7	74.4	67.8	70.3	86.6
	Ash	30.6	35.5	40.8	23.3	22.4	27.6	26.2	11.1
Elementa analysis (%)	Carbon	61.7	62.3	56.4	68.9	77.7	69.6	69.9	84.3
	Hydrogen	0.88	0.54	1.02	0.95	1.03	0.75	0.96	0.87
	Oxygen	1.39	1.68	1.81	1.45	1.14	1.51	1.16	0.43
	Nitrogen	0.45	0.24	0.58	0.57	0.56	0.53	0.54	0.46
	Sulfur	0.62	0.04	0.90	0.82	0.00	0.00	0.76	0.23
Components * (%)	SiO_2	49.1	48.7	48.2	43.8	44.5	44.4	49.3	42.8
	Al_2O_3	21.5	21.1	22.7	21.9	20.9	19.3	21.4	22.7
	Fe_2O_3	11.1	8.45	11.0	17.5	15.6	11.7	10.2	13.7
	K_2O	9.28	10.2	10.5	7.37	9.43	11.1	10.8	8.42
	TiO_2	5.70	5.15	5.16	5.00	6.76	6.80	6.09	9.30
	CaO	2.09	4.81	1.30	2.41	1.80	4.74	1.54	2.19
	MgO	0.33	0.93	0.31	0.38	0.35	0.70	N.D	N.D
	P_2O_5	N.D	0.32	0.25	0.39	0.38	0.29	0.29	0.65
	SO_3	0.80	0.37	0.50	1.12	N.D	0.68	0.28	N.D
	MnO	0.12	N.D	N.D	0.14	0.15	0.12	N.D	N.D
	ZrO_2	N.D	N.D	0.11	N.D	0.15	0.11	0.11	0.16
	SrO	N.D	N.D	N.D	N.D	N.D	0.09	N.D	N.D
	sum	100.0	100.0	100.0	100.0	100.0	100.0	100.0	100.0

* Each element was measured by XRF using ash sample of proximate analysis.

3.2. Thermal Properties

Figure 1 compares the TGA curves for anthracite before and after froth flotation. Unlike other carbon precursors, anthracite demonstrates minimal weight reduction due to its elevated degree of carbonization. This results from production conditions involving high temperatures and pressures, which give anthracite its distinctive dense structure and reduced volatile content, distinguishing it from other coal types, such as peat, lignite, and bituminous coal. However, noticeable disparities in weight loss emerge when comparing pre- and post-froth flotation states. Before flotation, samples WS and KD exhibit reduced weight loss starting around 100 °C, with an 8–9% reduction observed up to approximately 600 °C. Conversely, the floating-selected samples (WSF and KDF) show a more modest 2–3% reduction up to 700 °C, followed by a decrease of approximately 4–5% between 700 and 1000 °C. Notably, the volatile content, as detailed in Table 1, undergoes a significant reduction post froth flotation, with an overall decrease of approximately 43 to 64% compared to the raw samples. This trend is further validated by slightly lower weight reduction within the 100 to 700 °C range observed in sample WS, which initially had a higher volatile content among the four raw anthracite materials. It is important to consider that the floating process pulverizes the anthracite to around 60 mesh (approximately 210 μm), suggesting that some volatiles are released during the grinding process. This insight indicates that the mechano-chemical effect induced during grinding contributes to the removal of volatiles associated with the reduced fixed carbon.
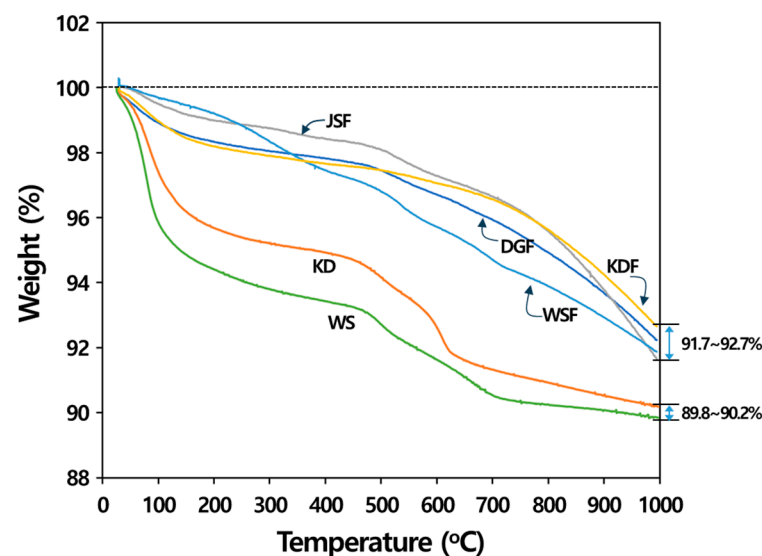

Figure 1. TGA curves for anthracites before (WD, KD) and after (JSF, DGF, WSF, KDF) froth flotation.

3.3. Production of Activated Carbon by Activation Methods

3.3.1. Physical Activation

The yield of activated carbon derived from anthracite decreased as the activation time increased. Notably, this reduction in yield for anthracite occurred at a more gradual pace compared to other carbon precursors that underwent prolonged activation reaction times. When examining photo images of the activated anthracite-based carbon, no distinct characteristics were observed, except for some grayish sections in the anthracite-H-10-2H sample (Figure 2f). This observation suggests that elevated temperatures and extended reaction durations led to carbon structure oxidation, potentially accelerated by the presence of residual ash [33].
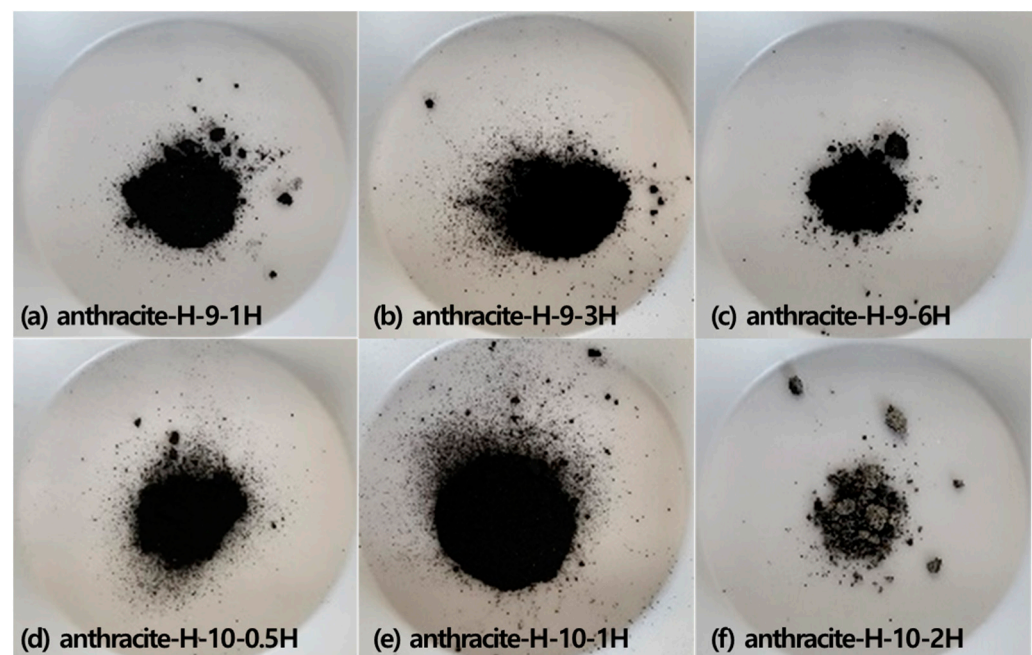
Figure 2. Photo images of anthracite-derived activated carbons under various physical activation conditions.

The nitrogen isotherm illustrated that a sample subjected to relatively short reactions at 900 °C and 1000 °C showcased a typical Type I isotherm, indicative of well-developed micropores (Figure 3). Nevertheless, as activation time increased, the proportion of mesopores gradually increased, and conditions of excessive activation seemed to contribute to the distortion of the carbon structure. These trends were also reflected in the specific surface area and total pore volume (Table 2). Activated carbon derived from anthracite exhibits distinct characteristics influenced by reaction conditions. As shown in Figure 3, it typically follows a Type I isothermal line. These characteristics become evident quite rapidly, regardless of the activation temperature, although the extent of the effect varies with different reaction conditions. However, as the reaction time increases, there is a significant reduction in the specific surface area of this activated carbon, leading to a sharp decline in yield, irrespective of the temperature used. The specific surface area and total pore volume of the activated anthracite ranged from 9 to 670 m^2/g and 0.03 to 0.39 cm^3/g, respectively, with production yields ranging from 21.3% to 83.7%. Notably, samples activated at a relatively low temperature of 900 °C, such as anthracite-H-9-3H, reach a maximum specific surface area of 600 m^2/g with a yield of 46%. However, further extending the reaction time beyond this point does not result in an increase in the specific surface area or pore volume; instead, these parameters decrease. Particularly noteworthy is the gradual increase in the proportion of mesopores, which becomes more pronounced. For example, compared to anthracite-H-9-1H, anthracite-H-9-3H exhibits a mesopore volume that **is** more than double, at 44.4% (Table 2). These distinctive characteristics are similarly observed in samples activated under 1000 °C. Therefore, it is evident that excessive activation conditions induce changes in pore structure, often accompanied by the collapse of the carbon lattice. Noteworthy is the anthracite-H-10-2H sample, displaying a non-porous pore structure with a specific surface area of 9 m^2/g. This implies that this phenomenon is more linked to the lingering ash content in anthracite rather than a mere collapse of the carbon structure due to excessive oxidation.
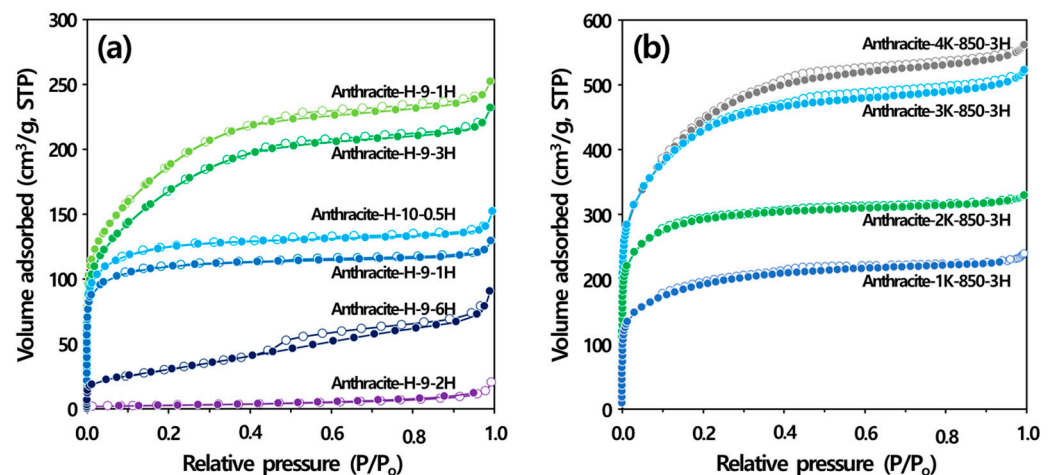
Figure 3. N$_2$/77K adsorption isotherm curves of anthracite-derived activated carbons; (**a**) physical and (**b**) chemical activation. Solid dots indicate adsorption characteristics, while empty dots represent desorption.

Table 2. Textural properties of anthracite-derived activated carbons under various physical activation conditions.

	Sample ID	S$_{BET}$ (m^2/g)	V$_{Total}$ (m^3/g)	V$_{Micro}$ (m^3/g)	V$_{Meso}$ (m^3/g)	VF$_{\_Meso}$ * (%)	Activation Yield (%)
Physical activation **	Anthracite-H-9-1H	420	0.200	0.160	0.040	20.0	83.7
	Anthracite-H-9-3H	600	0.360	0.200	0.160	44.4	46.0
	Anthracite-H-9-6H	110	0.140	0.040	0.100	71.4	21.3
	Anthracite-H-10-0.5H	470	0.230	0.180	0.050	21.7	79.6
	Anthracite-H-10-1H	670	0.390	0.230	0.160	41.0	54.6
	Anthracite-H-10-2H	9	0.030	0.000	0.030	100	22.3
Chemical activation ***	Anthracite-1K-850-3H	616	0.306	0.266	0.040	13.1	54.8
	Anthracite-2K-850-3H	963	0.421	0.386	0.036	8.55	59.1
	Anthracite-3K-850-3H	1381	0.669	0.592	0.077	11.5	31.9
	Anthracite-4K-850-3H	1413	0.719	0.644	0.075	10.4	21.5

* VF$_{\_Meso}$: Volume fraction of mesopores (=V$_{Meso}$/V$_{Total}$). ** Precursor-activation agent (H$_2$O)-activation temperature-activation time (hour). *** Precursor-activation agent (KOH)-activation temperature-activation time (hour).

Unlike the carbon structure, ash does not participate in pore formation during the reaction; instead, it encourages carbon oxidation reactions. The combination of a temperature of 1000 °C and a 2-h reaction time (anthracite-H-10-2H) suggests that only the remaining ash in anthracite after the reaction remains as a product. This interpretation is consistent with the observations depicted in Figure 2. Moreover, the yield of anthracite-H-10-2H was approximately 22%, closely resembling the yield of the anthracite used in the experiment, further reinforcing this interpretation.

In the realm of physical activation, oxidation initially occurs in the amorphous regions rather than the crystalline regions of the precursor's crystal grains. This mechanism leads to the development of micropores on the carbon surface via amorphous region oxidation. Subsequently, the oxidation reaction extends to the edges of the crystalline structure, resulting in the amplification of meso- and macro-pore volumes. These trends are evident in Table 2 and Figure 3a, where the volume of meso-pores ranges from 0.04 to 0.05 cm^3/g at yields up to 80%. However, as yields elevate to approximately 46–55%, the volume of meso-pores more than triples. This implies that activated carbon derived from anthracite primarily augments micropore volume through the oxidation of amorphous regions up to 80% yield. Later, the oxidation of crystalline edges contributes to a simultaneous increase in micropore and mesopore volumes. Despite these findings, the relatively lower specific

surface area of activated carbon derived from anthracite might be attributed to the lower amorphous content arising from the distinctive textile structure of anthracite.

3.3.2. Chemical Activation

In contrast to physical activation, this study provides compelling evidence that elucidates the interplay between specific surface area and two critical factors within the chemical activation process: reaction time and the quantity of agent used [23–25,34,35]. Across KOH/anthracite weight ratios of up to 4.0, all samples demonstrated typical Type I isotherms, revealing well-developed micropores alongside relatively high surface area and production yield (Figure 3b, Table 2). As consistent with prior research [34,35], the specific surface area of the carbon precursor increases with prolonged activation times and higher agent quantities (Figure 4). However, it is imperative to acknowledge that excessively prolonged reaction times can lead to a decline in specific surface area, as shown in Figure 4a. For instance, maintaining the activation process for 3 h results in a specific surface area of 1465 m^2/g, signifying a 16% increase compared to 1-h activation. Nevertheless, extending the activation period to 5 h shows a decrease in specific surface area to 236 m^2/g. Consequently, the production yield experiences a notable drop, decreasing from 55.8% to 47.8% as the activation time extends. This observation implies that the etching process and the broadening of carbon matrix pores persist even within dense and relatively crystalline structures due to the inherent nature of KOH activation.
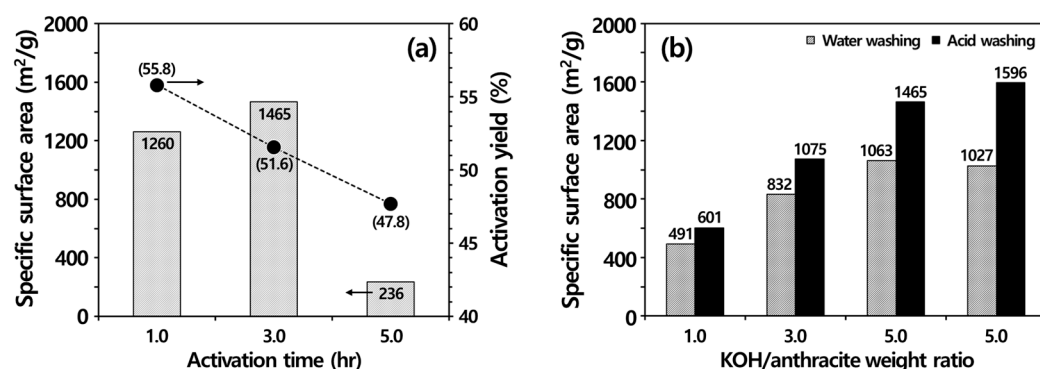

Figure 4. Effect of activation times (**a**) and quantity of chemical agent (**b**) on surface area development. All experiments were performed under an activation temperature of 850 °C. Arrows in the figure represent the data referring to each of scale bars.

The specific surface area of the activated sample also displays a discernible correlation with the quantity of the chemical agent employed (Figures 3b and 4b). Nevertheless, it is noteworthy that augmenting specific surface area through greater activator injection has an insignificant impact under KOH/anthracite weight ratios of 3.0 or higher. In comparison to the surface area of 1465 m^2/g achieved with a KOH/anthracite ratio of 3.0, even with increased KOH injection (KOH/anthracite ratio of 4.0), the specific surface area experiences only a modest additional increment of approximately 8.9%, reaching up to 1596 m^2/g.

The specific surface area of activated carbon derived from anthracite manifests substantial variation based on the employed washing method, as elucidated in Figure 4b. Water washing can obstruct carbon surface pores due to the presence of unremoved chemical agents, resulting in diminished specific surface area. Conversely, acid cleaning, entailing a more thorough purification process, augments the specific surface area while sacrificing yield by up to 30%. Despite the yield reduction, acid washing consistently boosts the specific surface area, with growth rates exceeding 20%. It is pertinent to recognize that the precise growth rate may fluctuate based on the KOH/anthracite ratio; however, on average, water washing shows surface area growth rates surpassing 20%. These findings emphasize the challenge of effectively eliminating persisting alkali metals post-activation solely through water washing. Therefore, it is imperative to incorporate acid washing as an additional step to remove residual ashes. The process of acid washing followed by

activation plays a key role in enhancing the specific surface area of activated carbon by alleviating the pore-blocking effects of remaining chemical agents.

3.4. Ash Removal Properties during Chemical Activation

Given the elevated ash content inherent in anthracite, various techniques, including physical, chemical, and microbial treatments, have been employed to reduce ash presence in anthracite [36–40]. Among these approaches, acid and alkali leaching have emerged as prominently efficient methods. Alkali leaching, in particular, has demonstrated exceptional efficacy, achieving treatment efficiencies surpassing 90% by initiating a dissolution reaction targeting quartz and aluminosilicate minerals. Recent investigations have utilized alkali leaching to extract valuable metals from coal ash. For instance, Pan et al. [31] accomplished the extraction of Si and Al utilizing alkali agents, while Motlagh et al. [32] effectively recovered biochar and SiO_2 through KOH activation of rice husks, which contained substantial amounts of Si (12–20 wt%) and carbon (30–50 wt%). These methodologies leveraged the chemical properties of Si and Al to facilitate the demineralization of crystalline minerals within alkaline environments. In light of these findings, it is conceivable that the KOH activation process applied in this study had the potential to remove Si and Al, which constitute the primary ash constituents in anthracite.

3.4.1. XRD

Despite undergoing froth flotation, anthracite still retains a substantial ash content, as evidenced by both surface characteristics and mineralogical analysis. Figure 5 illustrates the XRD results derived from the examination of anthracite employed in this study. The XRD peak reveals a consistent presence of identified minerals regardless of the collection area. The primary constituents include kaolinite, quartz, and muscovite, which are findings that align with previous research [39,40]. Furthermore, Davaadorj et al. [41] conducted an XRD analysis at the Jangseong mining site in Korea, identifying quartz, kaolinite, and muscovite, thereby highlighting their potential elimination through froth flotation. Nonetheless, these silicate minerals, persisting post froth flotation, likely contribute to the ash content of Si and Al within anthracite.
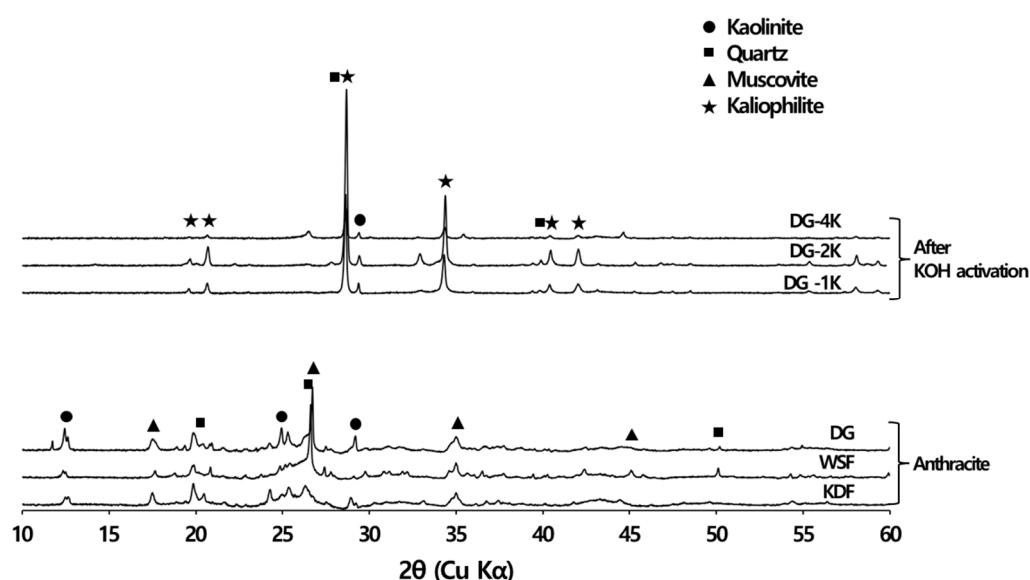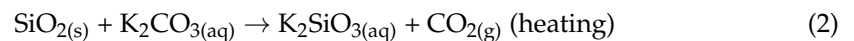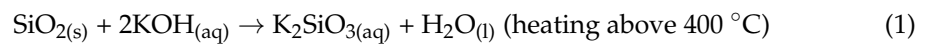

Figure 5. Changes in XRD peak patterns before (DG, WSF, KDF) and after (DG-1K, DG-2K, DG-4K) KOH activation.

Intriguingly, following chemical activation, these mineral peaks diminished, while the presence of kaliophilite ($KAlSiO_4$) was consistently identified regardless of the chemical agent quantity. Kaliophilite, as a secondary mineral, is commonly synthesized in alkaline

environments. Its well-known thermal stability and relatively low water solubility indicate that it would remain intact during water washing [42,43].

However, this observation shows that the alkali-rich environment during KOH activation facilitates the demineralization of silicate minerals, such as kaolinite, mullite, and quartz, leading to their transformation into amorphous forms. The reaction mechanisms of SiO_2 during the activation process using KOH and K_2CO_3 as activators are summarized in Equations (1) and (2):

$$SiO_{2(s)} + 2KOH_{(aq)} \rightarrow K_2SiO_{3(aq)} + H_2O_{(l)} \text{ (heating above 400 } ^\circ C) \tag{1}$$

$$SiO_{2(s)} + K_2CO_{3(aq)} \rightarrow K_2SiO_{3(aq)} + CO_{2(g)} \text{ (heating)} \tag{2}$$

Research by Nayak et al. [44] has documented that SiO_2 reacts with KOH and K_2CO_3 to generate K_2SiO_3 compounds, mirroring the transformation of quartz into $NaAlSiO_4$ and Na_2SiO_4 through reactions with Na_2CO_3 [31].

3.4.2. SEM-EDS

The SEM-EDS images conclusively substantiate the previously discussed observations conclusively (Figure 6). These images provide a detailed examination of particles larger than 60 mesh, obtained through froth flotation. Upon examination of individual particles, it becomes evident that ultrafine micrometer-range particles adorn the surface of parent particles. EDS analysis reveals Si and Al as the principal elements detected on the anthracite surface. The mapping images of each element show that these constituents cluster at specific points rather than uniformly scattering across the anthracite surface. This distinctive pattern is particularly evident in anthracite samples with high ash content (WS). Nevertheless, similar patterns appear in samples with relatively low ash content (KD). While there are locations where each element attains distinct high concentrations, there are also regions where elevated concentrations of Al and Si coincide. This observation implies that the ash components within anthracite predominantly take the form of minerals, aligning seamlessly with the images derived from XRD analysis. However, subsequent to KOH activation, the particles transform into intricately intertwined ultrafine structures on the micrometer scale, diverging from their raw counterparts.
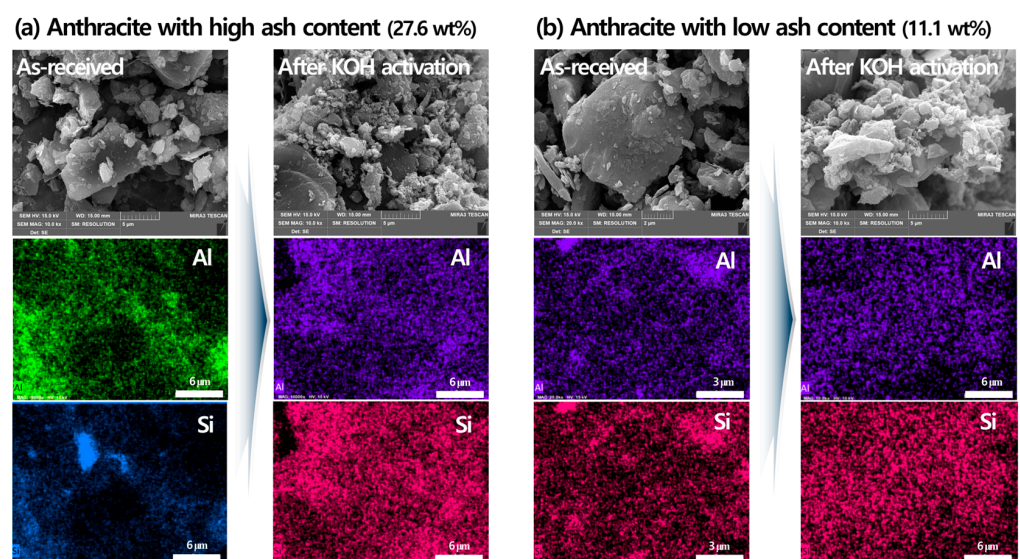

Figure 6. Graphical distribution images of aluminum and silicon were obtained before and after KOH activation using SEM-EDS, showing samples with relatively high (27.6 wt%) and low (11.1 wt%) ash contents. The SEM-EDS images were captured at a magnification of 10,000X and an acceleration voltage of 15 kV.

Additionally, the mapping results obtained from SEM-EDS analysis continue to unveil Al, Si, and Fe as predominant components. However, in stark contrast to the raw materials, these elements disperse across the sample, avoiding concentration at specific points. The content of these elements within the activated sample markedly diminishes compared to the raw materials. This diminution suggests that these ash constituents were readily dissolved during the ensuing washing phase. This dissolution process, combined with the uniform dispersion of Al and Si throughout the activated sample, hints at the demineralization of crystalline minerals inherent in anthracite during the KOH activation process.

3.4.3. Importance of Acid Washing after KOH Activation

Figure 7 offers a comparison of the ash reduction of anthracite using different treatments. Method I illustrates ash reduction conducted before activation, while methods II and III were applied post KOH activation. The ash content in anthracite subjected to acid treatment before activation stands at 21.6 wt%, with an associated removal rate of approximately 16.7%. Conversely, in the case of the activated sample, the ash removal efficiency (Method II: 37.9%, Method III: 67.0%) surpasses that of the acid-treated sample. Furthermore, the ash reduction rate subsequent to activation displays variation contingent upon the employed solution type. Rinsing the activated sample with tap water culminates in an ash removal rate of about 38%, more than twice the rate achieved through acid pretreatment. Remarkably, aluminum, the predominant ash component within anthracite, demonstrates distinct leaching characteristics rooted in its crystalline form. Amorphous aluminum is readily extracted via acid leaching, whereas Al incorporated into crystalline configurations, such as silicate minerals, exhibits greater resistance to acid leaching. Earlier studies have indicated that the extraction of Al from mullite can be accomplished through appropriate heat treatment in the presence of a sufficient flux, followed by acid leaching [31]. Consequently, the chemical activation via KOH initiates the dissolution of silicate minerals, primarily existing in crystalline states within a potent alkaline environment, thereby facilitating their elimination during the subsequent washing step. This mechanism stands in contrast to physical activation, which focuses solely on pore generation. In contrast, the chemical activation process orchestrates the concurrent initiation of pore development and ash reduction, utilizing a diluted acid solution as an integral component of the washing procedure.
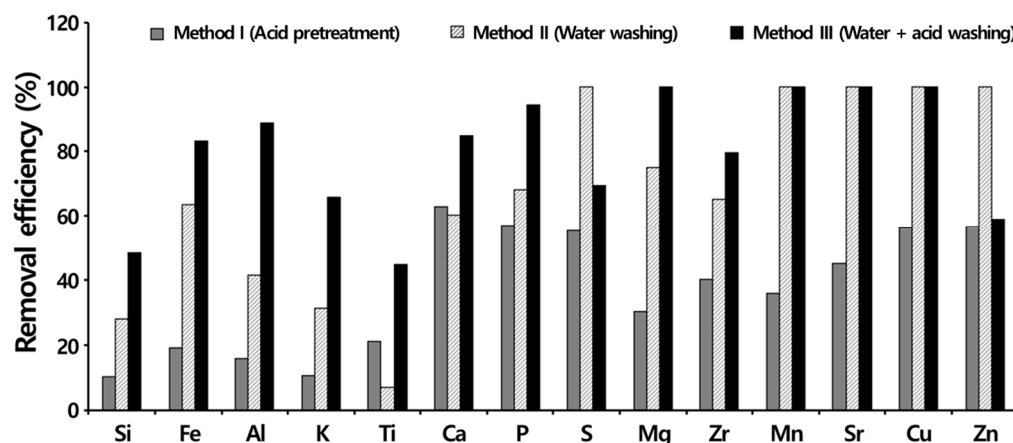

Figure 7. Ash removal efficiency of activated carbon derived from anthracite with various treatments.

4. Conclusions

In this study, we employed KOH chemical activation to concurrently regulate pore formation and ash content with the aim of efficiently producing activated carbon derived from high ash-containing anthracite in Korea. Unlike the physical activation method, the KOH activation process demonstrated notable efficiency in reducing specific surface area and ash content. Notably, KOH activation led to an increase in specific surface area due

to the introduction of the activating agent (KOH), resulting in a substantial production yield (62%). Under the conditions of a KOH-to-anthracite ratio of 4.0, a remarkable specific surface area of 1596 m^2/g was achieved.

Of particular significance is the post-KOH activation alteration in the composition of anthracite ash, encompassing elements such as Si, Al, Ti, and others. These components, which are prominent in anthracite ash, exhibited a substantial reduction of 54% to 65%. The evidence supporting this reduction in ash content was observed through XRD and SEM-EDS. This reduction in ash content is attributed to the effect of KOH, which acts as an activator capable of inducing the phase transition of constituent minerals like quartz, muscovite, and kaolinite—predominantly comprised of Si and Al. This transition led to the formation of kaliophilite. Notably, the ash reduction exhibited variability based on the washing method employed. Remarkable results were observed in the pickled sample, where Si and Al, constituents of silicate minerals, exhibited increased solubility in a potent alkaline environment. Consequently, these elements were effectively removed during the washing process.

In summation, the utilization of KOH chemical activation for anthracite-based activated carbon production presents a promising avenue for tailoring pore structure and reducing ash content. The effectiveness of KOH in modulating the composition of ash constituents highlights its pivotal role in enhancing the functional attributes of activated carbon. Moreover, the findings emphasize the influence of washing techniques on ash reduction, with Si and Al displaying increased susceptibility to removal within an alkaline environment.

References

1. Diercks, R.; Arndt, J.D.; Freyer, S.; Ceier, R.; Machhammer, O.; Schwartze, J.; Volland, M. Raw material changes in the chemical industry. *Chem. Eng. Technol.* **2008**, *31*, 631–637. [CrossRef]
2. Tost, M.; Hitch, M.; Chandurkar, V.; Moser, P.; Feiel, S. The state of environmental sustainability consideration in mining. *J. Clean. Prod.* **2018**, *182*, 969–977. [CrossRef]
3. Zhou, H.; Bhattarai, R.; Li, Y.; Dong, X.; Wang, T.; Yao, Z. Towards sustainable coal industry: Turning coal bottom ash into wealth. *Sci. Total Environ.* **2022**, *804*, 149985. [CrossRef] [PubMed]
4. Trinks, A.; Scholtens, B.; Mulder, M.; Dam, L. Fossil fuel divestment and portfolio performance. *Ecol. Econ.* **2018**, *146*, 740–748. [CrossRef]
5. Gueye, E.H.M.; Badri, A.; Boudreau-Trudel, B. Sustainable development in the mining industry: Towards the development of tools for evaluating socioeconomic impact in the Canadian context. *Environ. Dev. Sustain.* **2021**, *23*, 6576–6602. [CrossRef]
6. Li, Y.; Chiu, Y.H.; Lin, T.Y. Coal production efficiency and land destruction in China's coal mining industry. *Resour. Policy* **2019**, *63*, 101449. [CrossRef]
7. Gui, X.; Liu, J.; Cao, Y.; Miao, Z.; Li, S.; Xing, Y.; Wang, D. Coal preparation technology: Status and development in China. *Energy Environ.* **2015**, *26*, 997–1014. [CrossRef]
8. Xu, J.; Gao, W.; Xie, H.; Dai, J.; Lv, C.; Li, M. Integrated tech-paradigm based innovative approach towards ecological coal mining. *Energy* **2018**, *151*, 297–308. [CrossRef]
9. Zhao, S.; Alexandroff, A. Current and future struggles to eliminate coal. *Energy Policy* **2019**, *129*, 511–520. [CrossRef]
10. Lozano-Castello, D.; Lillo-Rodenas, M.A.; Cazorla-Amoros, D.; Linares-Solano, A. Preparation of activated carbons from Spanish anthracite. I. Activated by KOH. *Carbon* **2001**, *39*, 741–749. [CrossRef]

11. Cuhadaroglu, D.; Uygun, O.A. Production and characterization of activated carbon from bituminous coal by chemical activation. *Afr. J. Biotechnol.* **2008**, *7*, 3703–3710.

12. Zhao, C.; Ge, L.; Mai, L.; Li, X.; Chen, S.; Li, Q.; Li, S.; Yao, L.; Wang, Y.; Xu, C. Review on coal-based activated carbon: Preparation, modification, application, regeneration, and perspectives. *Energy Fuels* **2023**, *37*, 11622–11642. [CrossRef]

13. DeBarr, J.A.; Lizzio, A.A.; Daley, M.A. Adsorption of SO_2 on bituminous coal char and activated carbon fiber. *Energy Fuels* **1997**, *11*, 267–271. [CrossRef]

14. Zhao, H.; Wang, L.; Jia, D.; Xia, W.; Li, J.; Guo, Z. Coal based activated carbon nanofibers prepared by electrospinning. *J. Mater. Chem. A* **2014**, *2*, 9338–9344. [CrossRef]

15. Ye, R.; Xiang, C.; Lin, J.; Peng, Z.; Huang, K.; Yan, Z.; Cook, N.P.; Samuel, E.L.G.; Hwang, C.C.; Ruan, G.; et al. Coal as an abundant source of graphene quantum dots. *Nat. Commun.* **2013**, *4*, 2943. [CrossRef]

16. Zhang, Y.; Zhang, K.; Jia, K.; Liu, G.; Ren, S.; Lia, K.; Long, X.; Lia, M.; Qiu, J. Preparation of coal-based graphene quantum dots/α-Fe_2O_3 nanocomposites and their lithium-ion storage properties. *Fuel* **2019**, *241*, 646–652. [CrossRef]

17. Patney, H.K.; Nordlund, C.; Moy, A.; Rose, H.; Young, B.; Wilson, M.A. Fullerenes and nanotubes from coal. *Fuller. Sci. Technol.* **1999**, *7*, 941–971. [CrossRef]

18. Moothi, K.; Iyuke, S.E.; Meyyappan, M.; Falcon, R. Coal as a carbon source for carbon nanotube synthesis. *Carbon* **2012**, *50*, 2679–2690. [CrossRef]

19. Wu, L.; Liu, J.; Reddy, B.R.; Zhou, J. Preparation of coal-based carbon nanotubes using catalytical pyrolysis: A brief review. *Fuel Process. Technol.* **2022**, *229*, 107171. [CrossRef]

20. Qiu, J.S.; Zhou, Y.; Yang, Z.G.; Wang, D.K.; Guo, S.C.; Tsang, S.C.; Harris, P.J.F. Preparation of fullerenes using carbon rods manufactured from Chinese hard coal. *Fuel* **2000**, *79*, 1303–1308. [CrossRef]

21. Awasthi, S.; Awasthi, K.; Ghosh, A.K.; Srivastava, S.K.; Srivastava, O.N. Formation of single and multi-walled carbon nanotubes and graphene from Indian bituminous coal. *Fuel* **2015**, *147*, 35–42. [CrossRef]

22. Zhang, Y.; Lebedev, M.; Smith, G.; Jing, Y.; Bush, A.; Lalauer, S. Nano-mechanical properties and pore-scale characterization of different rank coals. *Nat. Resour. Res.* **2020**, *29*, 1787–1800. [CrossRef]

23. Kim, J.H.; Lee, G.; Park, J.E.; Kim, S.H. Limitation of K_2CO_3 as a chemical agent for upgrading activated carbon. *Processes* **2021**, *9*, 1000. [CrossRef]

24. Montes, V.; Hill, J.M. Activated carbon production: Recycling KOH to minimize waste. *Mater. Lett.* **2018**, *220*, 238–240. [CrossRef]

25. Hwang, S.Y.; Lee, G.B.; Kim, J.H.; Hong, B.U.; Park, J.E. Pre-treatment methods for regeneration of spent activated carbon. *Molecules* **2020**, *25*, 4561. [CrossRef]

26. Zou, X.; Ding, L.; Guo, X.L.; Lu, H.; Gong, X. Study on effects of ash on the evolution of physical and chemical structures of char during CO_2 gasification. *Fuel* **2018**, *217*, 589–596. [CrossRef]

27. Oglou, R.C.; Gokce, Y.; Yagmur, E.; Ghobadi, T.G.Y.; Aktas, Z. Highly stable megalopolis lignite based N and S self-doped hierarchically porous activated carbons for high performance supercapacitors and ash content effects on performance. *J. Energy Storage* **2022**, *46*, 103817. [CrossRef]

28. Yaman, S.; Yavuz, R. Stepwise demineralisation and chemical isolation of the mineral matter of Göynük lignite. *Energy Convers. Manag.* **2001**, *42*, 2119–2127. [CrossRef]

29. Meshram, P.; Purohit, B.K.; Sinha, M.K.; Sahu, S.K.; Pandey, B.D. Demineralization of low grade coal—A review. *Renew. Sustain. Energy Rev.* **2015**, *41*, 745–761. [CrossRef]

30. Parthasarathy, P.; Choi, H.S.; Park, H.C.; Hwang, J.G.; Yoo, H.S.; Lee, B.K. The review of upgrading coal techniques in South Korea. *J. Korea Soc. Waste Manag.* **2016**, *33*, 419–445. [CrossRef]

31. Pan, J.; Hassas, B.V.; Rezaee, M.; Zhou, C.; Pisupati, S.V. Recovery of rare earth elements from coal fly ash through sequential chemical roasting, water leaching, and acid leaching processes. *J. Clean. Prod.* **2021**, *284*, 124725. [CrossRef]

32. Motlagh, E.K.; Sharifian, S.; Asasian-Kolur, N. Alkaline activating agents for activation of rice husk biobar and simulated bio-silica extraction. *Bioresour. Technol. Rep.* **2021**, *16*, 100853. [CrossRef]

33. Peterson, C.A.; Brown, R.C. Oxidation kinetics of biochar from woody and herbaceous biomass. *Chem. Eng. J.* **2020**, *401*, 126043. [CrossRef]

34. Hilton, R.; Bick, P.; Tekeei, A.; Leimkuehler, E.; Pfeifer, P.; Suppes, G.J. Mass balance and performance analysis of potassium hydroxide activated carbon. *Ind. Eng. Chem. Res.* **2021**, *52*, 9129–9135. [CrossRef]

35. Romanos, J.; Beckner, M.; Rash, T.; Firlej, L.; Kuchta, B.; Yu, P.; Suppes, G.; Wexler, C.; Pfeifer, P. Nanospace engineering of KOH activated carbon. *Nanotechnology* **2012**, *23*, 015401. [CrossRef]

36. Ohm, T.I.; Chae, J.S.; Lim, J.H.; Moon, S.H. Evaluation of a hot oil immersion drying method for the upgrading of crushed low-rank coal. *J. Mech. Sci. Technol.* **2012**, *26*, 1299–1303. [CrossRef]

37. Rao, Z.; Zhao, Y.; Huang, C.; Duan, C.; He, J. Recent developments in drying and dewatering for low rank coals. *Prog. Energy Combust. Sci.* **2015**, *46*, 1–11. [CrossRef]

38. Nasir, S.; Kucerik, J.; Mahmood, Z. A study on the washability of the Azad Kashmir (Pakistan) coalfield. *Fuel Process. Technol.* **2012**, *99*, 75–81. [CrossRef]

39. Han, O.H.; Kim, M.K.; Kim, B.G.; Subasinghe, N.; Park, C.H. Fine coal beneficiation by column flotation. *Fuel Process. Technol.* **2014**, *126*, 49–59. [CrossRef]

40. Lu, G.; Zhang, K.; Cheng, F. The fusion characteristics of ahes from anthracite and biomass blends. *J. Energy Inst.* **2018**, *91*, 797–804. [CrossRef]
41. Davaadorj, T.; Baek, S.H.; Kim, B.G.; Jeon, H.S. Recovery of clean coal for the use of synthetic fuels from anthracite by forth flotation. *J. Korean Soc. Miner. Energy Resour. Eng.* **2018**, *55*, 285–292. [CrossRef]
42. Yao, Z.; Meisheng, X.; Ying, Y.; Lu, Z. Kaliophilite from fly ash: Synthesis, characterization and stability. *Bull. Mater. Sci.* **2011**, *34*, 1671–1674. [CrossRef]
43. Chen, X.; Chen, J.; Li, M.; Wang, J.; Zhou, Z.; Du, P.; Zhang, X. Synthesis of kaliophilite from high calcium fly ash: Effect of alkali concentration. *Case Stud. Constr. Mater.* **2022**, *17*, e01542. [CrossRef]
44. Nayak, P.P.; Nandi, S.; Datta, A.K. Comparative assessment of chemical treatments on extraction potential of commercial grade silica from rice husk. *Eng. Rep.* **2019**, *1*, e12035. [CrossRef]